RSC Advances

PAPER

View Article Online
View Journal | View Issue

Open Access Article. Published on 19 March 2025. Downloaded on 3/14/2026 12:22:18 PM.
This article is licensed under a Creative Commons Attribution-NonCommercial 3.0 Unported Licence.

Check for updates

Cite this: *RSC Adv.*, 2025, **15**, 8506

Reusing the expired Ceftazidime drug as an inhibiting agent for zinc metal corrosion in HCl medium†

Medhat M. Kamel, *[a] Safaa N. Abdou,[b] Zainab M. Anwar,[a] Magdy A. Sherif[a] and Nasser Y. Mostafa [a]

Drug disposal costs and drug-related environmental pollution could be reduced by reusing expired drugs. A well-known cephalosporin antibiotic that was listed as an essential medication by the World Health Organization is Ceftazidime. In this study, the corrosion mitigation properties of the expired Ceftazidime (CDZ) drug for zinc corrosion in 1 mol per L HCl solution were examined by weight loss (WL), frequency modulation (EFM), potentiodynamic polarization (PDP), and impedance spectroscopy (EIS) techniques. Theoretical calculations were carried out by Density Functional Tight Binding (DFTB) and Monte Carlo (MC) simulations. Furthermore, scanning electron microscopy (SEM) and energy dispersion X-rays (EDX) were used for examining the appearance and structure of the corroded zinc surface, respectively. For a CDZ concentration of 300 ppm, EFM techniques have shown an inhibitive efficiency (IE) of 70.3% at 298 K. The IE increased as the drug concentration increased from 50 to 300 ppm, whereas it reduced as the temperature increased. The inhibition effect ceased to improve at concentrations greater than 300 ppm. A mixed form of adsorption (physisorption and chemisorption) was suggested for inhibition. The adsorption process followed the Temkin model. The spontaneous character and exothermicity of the adsorption process were demonstrated by the ΔG°_{ads} and K_{ads} magnitudes. The PDP study demonstrated that CDZ was a mixed-type inhibitor as it retards both the cathodic and anodic reactions. According to EFM results, increasing the concentration of CDZ from 50 to 300 ppm reduces the corrosion current density from 163.5 to 78.7 μA cm^{-2}. SEM and EDX examinations revealed the adsorption of CDZ drug at the zinc surface. The DFTB and MC simulations revealed that the CDZ drug bonds to the zinc surface *via* the heteroatoms' lone pair of electrons and the pyridinium ring's π-electrons. The adsorption energy of the drug on the Zn surface was found to be −77.41 kJ mol^{-1}.

Received 27th January 2025
Accepted 10th March 2025

DOI: 10.1039/d5ra00650c

rsc.li/rsc-advances

1. Introduction

Metal corrosion is an internationally significant problem affecting both industrial and natural environments. It has a negative impact on the quality of the environment, industrial equipment, and infrastructure asset durability. Therefore, it is essential to design and implement corrosion protection techniques to minimize economic damage to materials, machinery, and buildings.[1,2]

Zinc is a valuable metal, having different uses in various fields. It is used to make a wide variety of alloys, coatings, and chemicals. Another typical use for it is to galvanize steel to prevent corrosion. Galvanized steel is used in the construction, automotive, and other industries. Because of its exceptional casting characteristics, Zn alloys are employed in die casting applications.[3–5] Both acidic and basic solutions can cause zinc to corrode. Within the pH range of 6.0 to 12.5 solutions, corrosion is relatively slow. Beyond this range, it is more prevalent.[6,7] Zinc metal corrodes in harmful conditions, resulting in white rust.[8] Zinc is susceptible to corrosion when subjected to industrial procedures, including scale removal and acidic solution cleaning. This makes zinc material inappropriate for use in industrial applications.[9–12] It has been established that using inhibitors is one of the best ways to prevent corrosion in metals.[13,14] These are chemicals that, by prohibiting the dissolution of metal, inhibit the corrosion of metallic substances.[15] The primary factor determining an inhibitor's efficacy is its capacity to absorb on a metal surface, resulting in substituting a water molecule at a corroding surface.[16]

Corrosion damage of zinc is commonly prevented through cathodic protection, utilizing galvanic or impressed current methods, often combined with paint or organic coatings. While

[a]*Department of Chemistry, Faculty of Science, Suez Canal University, Ismailia 41522, Egypt. E-mail: medhat_darwish@science.suez.edu.eg; Fax: +20 643230416; Tel: +20 1004482037*

[b]*Department of Chemistry, Khurmah University College, Taif University, Taif, Saudi Arabia*

† Electronic supplementary information (ESI) available. See DOI: https://doi.org/10.1039/d5ra00650c

 © 2025 The Author(s). Published by the Royal Society of Chemistry

Open Access Article. Published on 19 March 2025. Downloaded on 3/14/2026 12:22:18 PM.
This article is licensed under a Creative Commons Attribution-NonCommercial 3.0 Unported Licence.

polymer coatings offer a simple application, they provide less durable protection against environmental corrosion compared to cathodic protection techniques. Studies by Yasakau *et al.*[17] have shown that Layered Double Hydroxide (LDH) conversion coatings significantly enhance zinc's corrosion resistance. Specifically, LDH coatings incorporating vanadate resulted in a twenty-fold increase in impedance and a reduction in local ionic currents compared to uncoated zinc. This improved protection is attributed to the controlled release of vanadate anions from the LDH structure. The new study by Ouyang *et al.*[18] was explored on-site fabrication of biomimetic Slippery Liquid-Infused Porous Surfaces (SLIPS) coatings for zinc corrosion protection. A simple displacement reaction creates a dendritic zinc structure, which is then made superhydrophobic and infused with lubricant. This SLIPS coating significantly reduces corrosion current and enhances icing resistance, offering a practical, facile approach for field application.

To inhibit the deterioration of metals and alloys, several kinds of potent organic inhibitors are employed. These organic compounds have molecules with heteroatoms of N, O, and S, or structures with π-electrons. By covering the metal surfaces with a protective layer, these organic compounds inhibit the ionization of metals by blocking the diffusion of chemical species involved in the process.[19,20] Nevertheless, most of these organic inhibitors are pricey, hazardous, and harmful to the environment. This has encouraged researchers worldwide to investigate the potential of pharmaceuticals as corrosion inhibitors. Many studies have shown that using drugs as corrosion inhibitors is safe and has no effect on the surrounding environment. These findings have encouraged the application of medicines as corrosion inhibitors, which has led to the replacement of old, harmful corrosion inhibitors.[21]

When compared to industry-standard organic inhibitors, most drugs are more costly. Therefore, using a fresh drug as an anti-corrosion agent is not cost-effective. Thus, using the properties of expired medications to suppress corrosion is reasonable. Pharmaceuticals retain at least 90% of their original efficacy even after they have expired; nonetheless, their usage has been limited for therapeutic purposes due to liability issues and professional restrictions.[22] Utilizing expired medications could solve two more important problems, such as lowering drug-related environmental pollution and drug disposal expenses.[23,24]

Most of the inhibitors used to inhibit zinc corrosion were harmful, and an inhibitor's solubility in corrosive media is an important factor. To protect zinc from corroding, non-toxic pharmaceutical drugs are being used. Several drugs, including Guaifenesin,[25] Seroquel,[26] Clotrimazole,[27] Ketosulfone,[28] Floctafenine,[29] Hemorheologic,[30] Furosemide,[31] Telmisartan,[32] Paromomycin, Streptomycin, Spectinomycin,[33] Atenolol,[34] *N*-arylpyrroles,[35] Anisidines,[36] Gabapentin,[37] Erythromycin,[38] and Hexamine,[6] were used to prohibit zinc corrosion. The drugs, including Guaifenesin, Seroquel, Clotrimazole, and others, were tested in corrosive media such as HCl at varying concentrations and temperatures, as well as H_2SO_4. The inhibition efficiency, measured as a percentage, varied significantly depending on the drug, its concentration, and the specific corrosive environment. Clotrimazole exhibited the highest inhibition efficiency, reaching 90% at a concentration of 500 ppm in 0.1 mol per L HCl at 298 K, indicating its strong protective capabilities. In contrast, Ketosulfone displayed a significantly lower efficiency of 30% at 20 ppm in the same corrosive medium and temperature, highlighting its weaker inhibitory effect. Guaifenesin and expired Hemorheologic achieved 81% and 84% inhibition at 300 ppm in 2 mol per L HCl at 298 K and 0.1 mol per L HCl at 303 K, respectively, demonstrating comparable performance under different conditions. Seroquel reached 84% at 1000 ppm in 1 mol per L HCl at 333 K, while expired Gabapentin achieved 85% at 400 ppm in 0.1 mol per L HCl at 298 K. Floctafenine showed a 72% efficiency at 25 ppm in 0.1 mol per L HCl at 333 K. The efficiency of the other drugs ranged from 57% to 77% at varying concentrations and corrosive conditions, showing that concentration, temperature, and the composition of the corrosive medium play significant roles in the effectiveness of the drugs as corrosion inhibitors.

Because pharmaceutical compounds contain heteroatoms such as oxygen, sulfur, and nitrogen, they provide promising potential for inhibiting corrosion. Their large molecular sizes and great water solubility make this particularly intriguing.[39]

Table 1 The chemical structure, IUPAC name, molecular mass, and molecular formula of the expired Ceftazidime (CDZ) drug

Drug	Structural formula	Characteristics
Ceftazidime (CDZ)	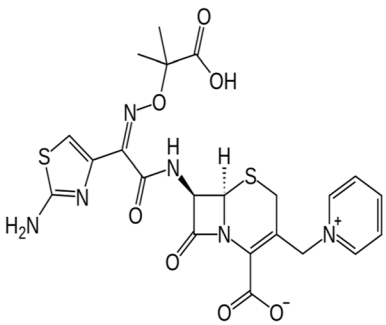	(6*R*,7*R*,*Z*)-7-(2-(2-Aminothiazol-4-yl)-2-(2-carboxypropan-2-yloxyimino)acetamido)-8-oxo-3-(pyridinium-1-ylmethyl)-5-thia-1-aza-bicyclo[4.2.0]oct-2-ene-2-carboxylate Molecular formula: $C_{22}H_{22}N_6O_7S_2$ Molecular mass: 546.58 g mol^{-1}

Open Access Article. Published on 19 March 2025. Downloaded on 3/14/2026 12:22:18 PM.
This article is licensed under a Creative Commons Attribution-NonCommercial 3.0 Unported Licence.

A third-generation cephalosporin antibiotic, Ceftazidime (CDZ) drug, is free of poisonous metallic components.[40,41] The CDZ drug is one of the most significant drugs that are crucial to treating various infections, including joint and vibrio infections, in the healthcare system. It contains many binding centers, such as atoms of N, S, and O. The inhibitive impact of the CDZ drug is usually attributed to the way it interacts with the metal surface *via* the adsorption process.[42] Table 1 shows the CDZ drug's structural formula, IUPAC identification, molecular mass, and molecular structure. Additionally, our earlier study on the effective inhibition of corrosion of copper metal using expired Ceftazidime[42] led us to employ Ceftazidime to suppress the corrosion of zinc, another essential industrial metal. Additionally, most of the characteristics needed to be employed as a corrosion inhibitor are present in CDZ, such as electron-rich heteroatoms (N, S, and O), electron-rich efficient groups (C=N, OH, NH, NH_2, C=O, COO^-, π-electrons of aromatic ring), good structure to cover the metal surface, and dissolved in water. Therefore, expired CDZ was used as an inhibitor in the current investigation to study zinc corrosion mitigation in a 1 mol per L HCl medium. The experiments were carried out using WL, PDP, EIS, and EFM methodologies. The composition and morphology of the zinc metal surface were investigated using EDX and SEM analyses. The drug's type of adsorption on zinc metal was evaluated using several adsorption isotherms. Additionally, the thermodynamic characteristics pertaining to the adsorption process were established. The mechanism of inhibition was investigated. The interaction between the CDZ molecules and the zinc surface was described by DFTB, MC, and computational studies.

2. Materials and methods

2.1 Zn strips

The corrosion rate was determined using high-purity 99.2% zinc metal strips (Cd 0.52%, Sn 0.07%, Pd 0.18%, Fe 0.035%, and Zn remaining). After the metal strips were abraded using 400, 800, 1500, and 2000 grade silicon carbide emery papers, they were cleaned with distilled water, degreased in acetone, and thoroughly dried.[43] Zinc strips measuring $2 \times 2 \times 0.1$ cm^3 were used for WL experiments in a 1 mol per L HCl solution. Electrochemical investigations were conducted using zinc strips with a 1 cm^2 exposure area. AR-grade HCl (32%) and double-distilled water were used to prepare the 1 mol per L HCl solution (blank). This concentration was chosen for its balance between inducing significant corrosion and maintaining a reasonable level of safety during experimentation.

2.2 Inhibitor

A stock solution containing 1000 mg L^{-1} (ppm) was prepared by dissolving 1 gram of expired CDZ medication (expired 1 year ago) in 1 Liter of bi-distilled water. The stock solution was then diluted with bi-distilled water to achieve concentrations ranging from 50 to 300 ppm. Different concentrations of CDZ were added to 1 mol per L HCl to create the corrosive medium. To determine if the Ceftazidime molecule degraded after expiration, FTIR spectroscopy was performed. The resulting spectra of both fresh and expired samples showed nearly identical patterns, indicating that the functional groups and overall chemical structure were preserved (Fig. S1, ESI†). No notable structural alterations or degradation products were observed.

2.3 WL measurements

According to ASTM-G1,[44] WL measurements were established. To conduct WL tests, cleaned zinc strips were immersed in 100 cm^3 blank solution having various CDZ concentrations for 6 hours. The studies were conducted between 298 and 318 K. The rusted Zn metal strips were removed after 6 hours, cleaned with distilled water, allowed to dry in acetone, and then weighed. Three sets of measurements were made, and the average value was recorded ± standard deviation.

2.4 Electrochemical studies

ASTM-G102 was followed for conducting the electrochemical tests.[24] The Gamry Instrument PCI4300 Potentiostat/Galvanostat ZRA was utilized to evaluate the potentiodynamic polarization (PDP), the impedance spectroscopy (EIS), and the frequency modulation (EFM) at 298 K. Experiments were conducted using a three-electrode system that included a working electrode (Zn strip with 1 cm^2 of exposure), an auxiliary electrode (Pt), and a reference electrode (saturated calomel). The zinc electrode was submerged in the corrosive medium for 30 minutes before each electrochemical measurement to allow the open circuit potential to achieve equilibrium. Polarization curves were obtained within the potential window of −0.3 to +0.2 V regarding the open circuit potential value (OCP) with a scan rate of 1 mV s^{-1}.

EIS studies were accomplished utilizing AC signals in the frequency range of 100 kHz to 0.5 Hz, with an amplitude of 10 mV s^{-1}. The ZSimp Win 3.21 program was used to fit all impedance values to the relevant equivalent circuits. Nyquist and Bode's plot provided the impedance parameters. The reproducibility of the EIS measurements was confirmed by performing triplicate experiments under identical conditions. The consistency of the obtained spectra and fitted parameters demonstrates the reliability of the data. The EFM investigation employed two frequencies, 2 and 5 Hz. Every second, the waveform renews itself at the shortest frequency of 100 mHz. The spectrum includes current actions caused by intermodification and harmonic current peaks. To compute the corrosion current, Tafel slopes (β_c and β_a), and causality factors (CF-2 and CF-3), the bigger peaks were used.

2.5 SEM studies

A scanning electron microscope (model: JOEL JSM-6510LV) was utilized to examine the surface morphologies of the zinc specimens. To conduct the studies, zinc specimens were submerged in a blank solution for 6 hours in the absence and presence of 300 ppm of the CDZ inhibitor. The metal samples were removed, washed with bi-distilled water, dried, and subjected to

 © 2025 The Author(s). Published by the Royal Society of Chemistry

Open Access Article. Published on 19 March 2025. Downloaded on 3/14/2026 12:22:18 PM.
This article is licensed under a Creative Commons Attribution-NonCommercial 3.0 Unported Licence.

SEM analysis. The accelerating beam used had a potential of 35 kV.

2.6 EDX analysis

The EDX device (model: EDX-FEI-QUANTA FEG 250) was used to investigate the chemical analysis of the zinc surface.

2.7 Modeling and computations

Chemical simulations were used to describe the adsorption mechanism. The inhibitory efficiency of the corrosion inhibitor was connected to the quantum chemical characteristics. In the quantum computing package, DFTB +1.3 is utilized. Slater–Koster file libraries provided the empirical parameters required for the DFTB integral evaluation computation. For the current system, Auorg parameters were employed.[45–47] Energy of the lowest unoccupied molecular orbital (E_{LUMO}), energy of the highest occupied molecular orbital (E_{HOMO}), adsorption energy (E_{ads}), and energy gap (ΔE) were among the thermodynamic and electronic characteristics that were computed to evaluate the effectiveness of the CDZ drug for inhibiting corrosion.

The preferred adsorption arrangements of the CDZ molecule on the adsorption centers of zinc's periodic structure were examined *via* MC simulation. Utilizing a simulated annealing algorithm, MC checks of possible substrate-adsorbate arrangements were conducted to find possible adsorption sites.[45] A periodic slab model box of a super unit cell with a 25 Å vacuum layer was used for MC to avoid interference between periodic unit cells. A single inhibitor molecule and a 20 Å vacuum layer in the *Z*-direction cover a zinc (002) supercell surface with 8 atomic layers. The mechanism of interactions between the drug and the zinc surface and the behavior of the CDZ molecule during adsorption were clarified by the compass field of force.

3. Results and discussion

3.1 WL tests

The WL studies were carried out with and without different concentrations of CDZ ranging from 50 to 300 ppm in a blank acid solution. Fig. 1 illustrates how the inhibition efficiency (IE_w) changes with the CDZ concentration at various temperatures. Zinc weight loss and corrosion rate (CR) decrease, and inhibition efficiency increases when CDZ is added to a 1 mol per L HCl solution. The results revealed that zinc corroded rapidly when exposed to a 1 mol per L HCl solution, while the rate of breakdown was slowed down when CDZ expired drug was present. Furthermore, an increase in inhibitory efficacy with concentration indicates a strong interaction between the drug and the zinc surface.[48] The results also revealed that CDZ drug might effectively block the Zn surface in a 1 mol per L HCl solution. Additionally, as demonstrated by Fig. 1, the efficiency of inhibition drops as the temperature gets higher, suggesting that some of the drug that was previously adsorbed may desorb at higher temperatures. This indicates that the CDZ molecules were physically coated on the zinc surface, and physisorption is the term for the adsorption process.[49]

The corrosion rate (CR) was computed by eqn (1).[50]

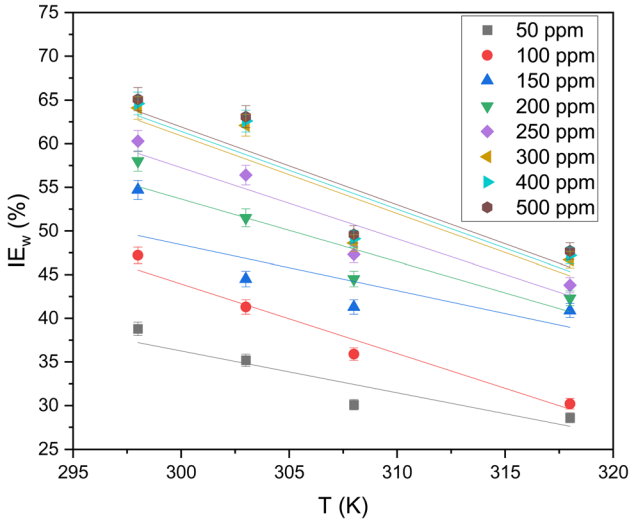

Fig. 1 Effect of temperature on IE_w at different concentrations of expired Ceftazidime drug for zinc corrosion in 1 mol per L HCl.

$$CR = \frac{\Delta W}{A \times t} \quad (1)$$

where ΔW is the WL of the Zn strips in mg, A is the area of the Zn strip in cm^2, and t is the submersion period in minutes. The inhibition efficacy (IE_w), and the surface coverage (θ) were determined by eqn (2).[51]

$$IE_w = \left(1 - \frac{W_{inh}}{W_{corr}}\right) \times 100 = \theta \times 100 \quad (2)$$

where W_{corr} and W_{inh} stand for the WL of zinc strips free of and with the drug, respectively.

θ is the surface coverage of zinc. Table 2 presents data for the corrosion inhibition of zinc in a blank solution by CDZ. The WL measurements were conducted 240 minutes at varying temperatures and CDZ concentrations. The data suggests that CDZ is an effective inhibitor for zinc corrosion in an acidic environment. The inhibition efficacy is influenced by both the quantity of CDZ and the temperature of the solution. The addition of CDZ to the solution significantly inhibits zinc corrosion. The WL and CR decrease with increasing CDZ concentration. The CR decreases to 10.62×10^{-3} mg cm^{-2} min^{-1} at 298 K when the medication exists with a concentration of 300 ppm. This indicates the drug's capability to develop a shielding film on the zinc surface. As temperature increases, the corrosion rate of zinc generally increases in both the absence and presence of CDZ. This is expected behavior as higher temperatures provide more energy for the corrosion process. As the inhibition efficiency did not improve beyond 300 ppm (Fig. 1), the electrochemical experiments were performed exclusively within the 50–300 ppm concentration range. The surface coverage and IE_w increase with increasing CDZ concentration. At 298 K, with 300 ppm of CDZ present, the IE_w reaches 64.1%. This suggests that the drug molecules are effectively adsorbing onto the zinc surface, blocking corrosive sites.

Open Access Article. Published on 19 March 2025. Downloaded on 3/14/2026 12:22:18 PM.
This article is licensed under a Creative Commons Attribution-NonCommercial 3.0 Unported Licence.

Table 2 Data of WL measurements at 240 min for zinc in a 1 mol per L HCl, in the absence and presence of different concentrations of the expired Ceftazidime drug at different temperatures

Temp. (K)	Dose of drug (ppm)	Weight loss (mg cm^{-2})	CR × 10^{-3} (mg cm^{-2} min^{-1})	Surface coverage (θ)	IE$_w$ (%)
298	0.00	7.11	25.45	—	—
	50	4.35	18.12	0.388	38.8 ± 0.1
	100	3.75	15.62	0.472	47.2 ± 0.3
	150	3.22	13.41	0.547	54.7 ± 0.2
	200	2.98	12.48	0.580	58.0 ± 0.3
	250	2.82	11.75	0.603	60.3 ± 0.2
	300	2.55	10.62	0.641	64.1 ± 0.1
303	0.00	8.22	34.25	—	—
	50	5.32	21.16	0.352	35.2 ± 0.2
	100	4.82	20.08	0.413	41.3 ± 0.1
	150	4.56	19.37	0.445	44.5 ± 0.3
	200	3.98	16.58	0.515	51.5 ± 0.2
	250	3.58	14.16	0.564	56.4 ± 0.3
	300	3.11	12.95	0.621	62.1 ± 0.1
308	0.00	9.70	38.29	—	—
	50	6.82	29.60	0.301	30.1 ± 0.2
	100	6.56	27.33	0.359	35.9 ± 0.3
	150	6.21	25.87	0.413	41.3 ± 0.1
	200	5.38	22.41	0.445	44.5 ± 0.2
	250	5.11	21.23	0.473	47.3 ± 0.4
	300	4.98	20.75	0.486	48.6 ± 0.3
318	0.00	10.65	49.79	—	—
	50	7.60	36.41	0.286	28 2 ± 0 28.6 ± 0.2
	100	7.24	35.08	0.320	30.2 ± 0.3
	150	6.38	33.41	0.409	40.9 ± 0.1
	200	6.14	32.55	0.423	42.3 ± 0.3
	250	5.98	36.81	0.438	43.8 ± 0.2
	300	5.78	29.50	0.467	46.7 ± 0.4

A comparison of Ceftazidime's corrosion inhibition with varying expiration dates revealed that two, and three-year expired samples performed poorly (Fig. S2 and S3, Tables S1 and S2 in ESI†). This led us to prioritize the one-year expired drug, which demonstrated the most effective inhibition.

Acid dissolves metal by an electrochemical reaction. Zinc dissolves at the anode, producing corresponding ions.[52]

$$Zn \rightarrow Zn^{2+} + 2e^- \quad (3)$$

In an aerated solution of acidic chloride, the reaction occurring in the cathodic area is:

$$H^+ + e^- \rightarrow H_{ads} \quad (4)$$

$$H_{ads} + H_{ads} \rightarrow H_2 \quad (5)$$

or

$$4H^+ + O_2 + 4e^- \rightarrow 2H_2O \quad (6)$$

Therefore, the overall corrosion reaction in an aerated solution will be:

$$2Zn + 4H^+ + O_2 \rightarrow 2H_2O + 2Zn^{2+} \quad (7)$$

3.2 Adsorption behavior and thermodynamic parameters

The adsorption phenomenon, in which inhibitor molecules prefer to adsorb on the corroding surface layer, has been proposed as the origin of corrosion inhibition. In this work, the extent of surface coverage occupied by CDZ molecules (θ) was

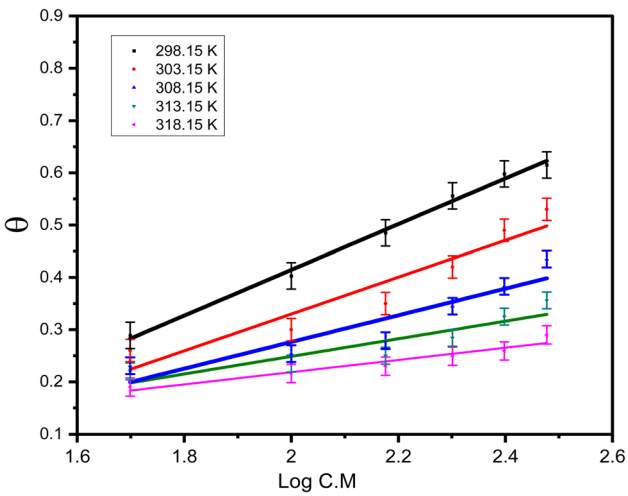

Fig. 2 Temkin adsorption curves for zinc in 1 mol per L HCl with different concentrations of CDZ at different temperatures (298–318 K).

 © 2025 The Author(s). Published by the Royal Society of Chemistry

Open Access Article. Published on 19 March 2025. Downloaded on 3/14/2026 12:22:18 PM.
This article is licensed under a Creative Commons Attribution-NonCommercial 3.0 Unported Licence.

Table 3 Adsorption parameters for zinc at various concentrations of the expired Ceftazidime drug at different temperatures in 1 mol per L HCl solutions

Temperature (K)	$\log K_{ads}$	K_{ads}	$-\Delta G^{\circ}_{ads}$ (kJ mol^{-1})
298	3.60	3981.07	30.49
303	3.00	1000.00	27.07
308	2.88	758.58	26.38
313	2.41	257.04	23.70
318	2.25	127.83	21.97

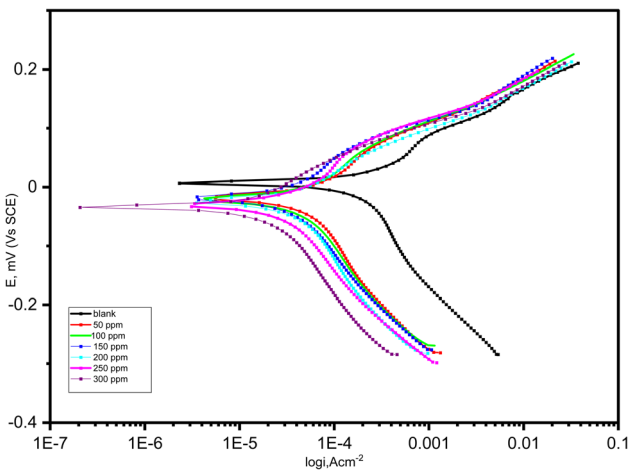

Fig. 3 Potentiodynamic polarization curves of zinc in 1 mol per L HCl without and with different concentrations of the Ceftazidime drug at 298 K.

computed by applying the traditional WL method to investigate the most appropriate adsorption mode. The Temkin model with high fitting (R^2 ranging between 0.990 and 0.997) was proposed (Fig. 2) to shed further light on the inhibitory effect of CDZ on the Zn surface. Eqn (8) was used to assess the Temkin model's applicability.[42]

$$\theta_{coverage} = \left(\frac{2.303}{a}\right)\log K_{ads} + \left(\frac{2.303}{a}\right)\log C \quad (8)$$

For this equation, C represents the CDZ drug concentration, a is a molecular interaction parameter, K_{ads} is the equilibrium constant, and θ is the fraction of surface covering ($\theta = IE_w/100$). A straight line having a slope of $(2.303/a)$ with an intercept of $[(2.303/a)\ \log K_{ads}]$ is established by plotting $\log C$ against θ (Fig. 2). Table 3 displays the values of K_{ads}. High values of K_{ads} indicate a strong and stable adsorbed film.[53] Rising temperatures cause the value of K_{ads} to drop. The physical nature of adsorption causes CDZ molecules to desorb from zinc surfaces more quickly at higher temperatures.

Eqn (9) was employed to obtain the standard free energy of adsorption, ΔG°_{ads}, which was linked to K_{ads} as previously established.[54,55]

$$K_{ads} = \exp\left(\frac{-\Delta G^{\circ}_{ads}}{RT}\right) \quad (9)$$

where T is the Kelvin temperature and R is the gas constant. The calculated ΔG°_{ads} of the CDZ medication at various temperatures (298–318 K) are shown in Table 3. The negative sign of ΔG°_{ads} refers to the adsorption process of the CDZ drug on the Zn surface being stable and spontaneous.[56] Moreover, some studies have discriminated against the chemisorption and physisorption processes using ΔG°_{ads} values.[57,58] The magnitudes of ΔG°_{ads} below 20 kJ mol^{-1} were linked to physisorption, or the interaction of electrostatic charges, whereas values above 40 kJ mol^{-1} were related to chemisorption, or the transfer of electrons between the drug molecules and the Zn surface. The CDZ medication has ΔG°_{ads} values ranging between −21.97 and −30.49 kJ mol^{-1} in the current investigation. Hence, rather than being a simple case of physisorption or chemisorption, the adsorption of the CDZ medication on the Zn surface is a complex combination of chemical and physical adsorption.[56]

3.3 PDP study

The PDP curves of the zinc electrode in a blank solution were displayed in Fig. 3 at a voltage scan rate of 1 mV s^{-1} and 298 K, without and with different CDZ drug concentrations. Electrochemical parameters, including corrosion current density (i_{corr}), corrosion potential (E_{corr}), and the cathodic and anodic Tafel slopes (β_c and β_a), were determined (Table 4) by applying the Tafel extrapolation method to the polarization curves shown in Fig. 3. The Tafel extrapolation method is a fundamental electrochemical technique used to determine corrosion parameters by analyzing a Tafel plot. This plot, which graphs the logarithm of current density against electrode potential, reveals distinct linear regions corresponding to anodic and cathodic reactions.

Table 4 Potentiodynamic polarization parameters of zinc in 1 mol per L HCl without and with different concentrations of the Ceftazidime drug at 298 K

[CDZ] (ppm)	$-E_{corr}$ (mV *vs.* SCE)	β_a (mV dec^{-1})	$-\beta_c$ (mV dec^{-1})	i_{corr} (μA cm^{-2})	θ	IE_p (%)
Blank	117	119	199	235	—	—
50	113	112	146	150	0.362	36.2 ± 0.2
100	111	107	127	123	0.476	47.6 ± 0.1
150	108	102	116	105	0.553	55.3 ± 0.1
200	106	99	112	93	0.604	60.4 ± 0.2
250	104	91	105	84	0.642	64.2 ± 0.4
300	100	78	87	73	0.689	68.9 ± 0.3

Open Access Article. Published on 19 March 2025. Downloaded on 3/14/2026 12:22:18 PM.
This article is licensed under a Creative Commons Attribution-NonCommercial 3.0 Unported Licence.

By extrapolating these linear regions, their intersection point provides the corrosion potential (E_{corr}) and corrosion current (i_{corr}). E_{corr} signifies the potential where anodic and cathodic reaction rates equalize, while i_{corr} directly correlates with the corrosion rate.[59] Furthermore, the slopes of these linear regions, known as Tafel slopes (β_c and β_a), offer insights into the kinetics of the electrochemical reactions. Essentially, Tafel extrapolation harnesses the linear behavior of electrochemical polarization curves to quantify corrosion rates and understand the underlying reaction mechanisms. The following equation was used to determine the percentage inhibition efficiency (IE_p).[60]

$$IE_p = \frac{i^{\circ}_{corr} - i_{corr}}{i^{\circ}_{corr}} \times 100 \quad (10)$$

i°_{corr} and i_{corr} stand for the corrosion current density in the absence and presence of the CDZ drug, respectively. Significant

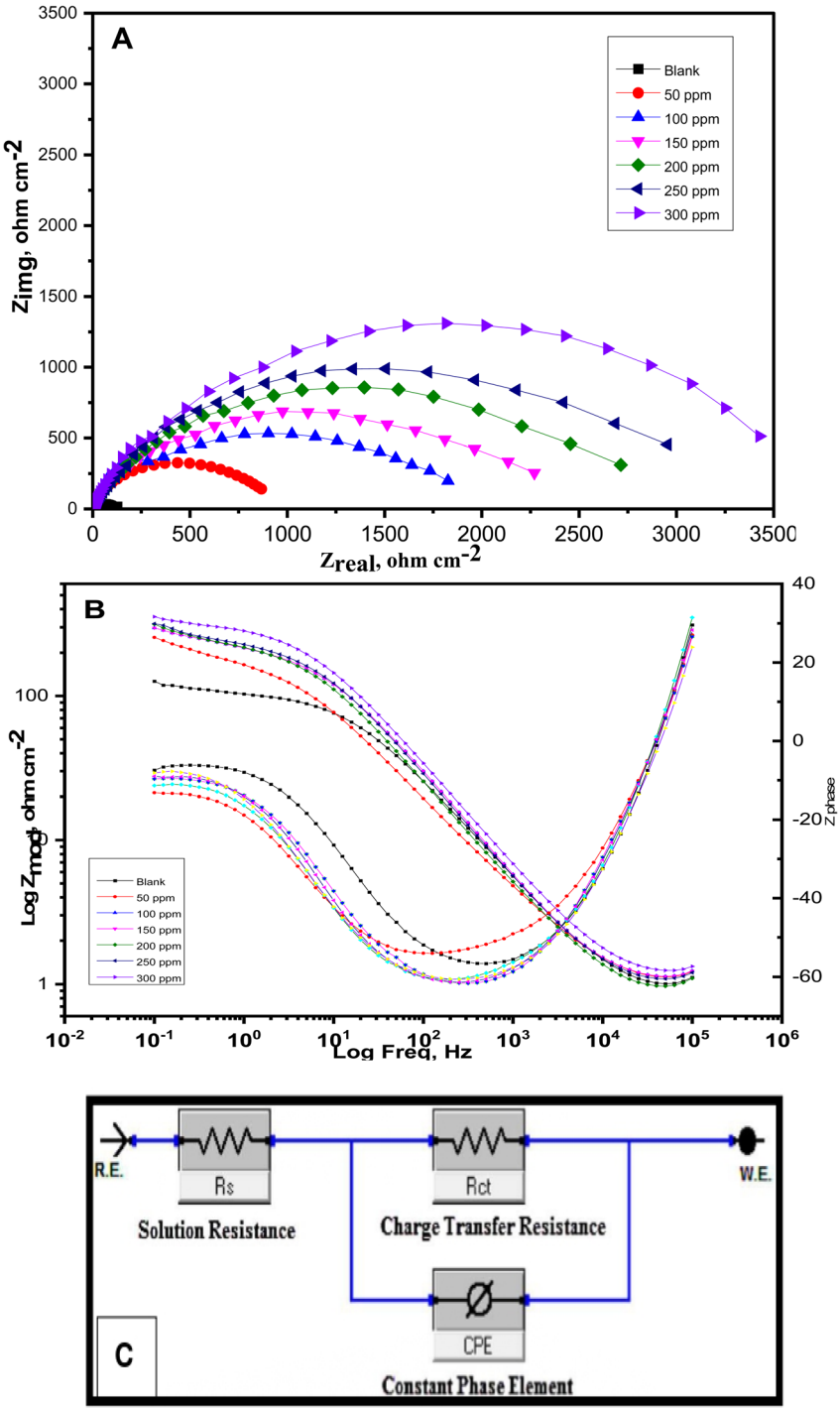

Fig. 4 Nyquist (A) and Bode (B) plots of zinc in 1 mol per L HCl without and with different concentrations of the expired Ceftazidime drug at 298 K, and (C) the equivalent circuit used to fit the EIS data.

 © 2025 The Author(s). Published by the Royal Society of Chemistry

Open Access Article. Published on 19 March 2025. Downloaded on 3/14/2026 12:22:18 PM. This article is licensed under a Creative Commons Attribution-NonCommercial 3.0 Unported Licence.

corrosion developed when the blank solution came into direct contact with zinc metal. Zinc dissolves more quickly in corrosive solutions when aggressive ions like Cl^- and H_3O^+ are present. The insertion of CDZ into the corrosive solution causes notable drops in current densities, which slowed the zinc's rate of corrosion. The anodic and cathodic sections of the measured polarization curves (Fig. 3) progressively shift toward lower current density as the concentration of CDZ increases, indicating a decline in the overall corrosion rate.[61] Anodic and cathodic branches' shapes were altered, demonstrating that the existence of CDZ controlled both anodic and cathodic processes. The cathodic polarization curves depict the evolution of hydrogen, but the dissolution of zinc is represented by anodic polarization curves.

In relation to the blank solution, the inhibitor acts as a mixed-type inhibitor if the E_{corr} is smaller than 85 mV and as a cathodic or anodic type if it is bigger than 85 mV. According to Table 4, there is a 17 mV difference between E_{corr} in the drug-containing solution (300 ppm) and the blank solution in this study, suggesting that the CDZ medication is a mixed inhibitor.[57] Tafel plots in Fig. 3 illustrate a positive shift in the corrosion potential (E_{corr}) relative to the drug-free blank solution. The polarization curves and collected data demonstrate that the drug influences both the anodic and cathodic half-reactions. Notably, both the anodic and cathodic current densities significantly drop in comparison to the blank solution, confirming that the CDZ drug functions as a mixed inhibitor.[62] Data shown in Table 4 demonstrates a substantial reduction in current density with the insertion of the CDZ medication. When the drug's concentration reaches 300 ppm, the efficiency of inhibition rises to 68.9%. As the quantity of CDZ drug in the blank solution increases, the β_a and β_c show a decrease in value. The possible reason for these effects could be the adsorption of CDZ molecules onto the zinc surface.[63]

3.4 EIS study

The Nyquist diagrams of zinc in blank solution free of and with varying CDZ medication doses were shown in Fig. 4A. For both the blank and CDZ drug solutions, the Nyquist diagrams display only one semicircle of depressed capacitance. Electrodes that show frequency dispersion because of surface defects and other inhomogeneities of the metal were characterized by depressed semicircles, which correlate to Nyquist diagrams.[64] The Zn corrosion reaction was thought to be controlled by a single charge transfer process, as indicated by the singular capacitive loop.[64] In accordance with the polarization study, this shape remained unchanged with the presence of CDZ at various dosages, indicating that the process of corrosion is under activation control and does not alter.[65] It is worth observing that the centers of the depressed semicircles were laid under the *X*-axis. The frequency dispersion can cause this phenomenon. The influence of the inhomogeneous Zn surface and the interfacial impedance on frequency dispersion could be the reason for this behavior.[66] Usually, the presence of inhibitor adsorption and coarseness/roughness is the cause.[67,68] Furthermore, compared to a free HCl solution, the existence of CDZ medication increased the diameter of the capacitive loops, indicating that the drug inhibits zinc metal from corroding by covering the zinc metal's surface with a barrier coating.[69]

Because of the inhomogeneities of the metal surface, the Bode plot shown in Fig. 4B generally produces a depressed semicircle for the metal-solution interface. Zinc corrosion in acidic conditions increases the metal's surface roughness, which lowers the phase angle.[26] The phase angle increased as drug concentration increased, as shown by the Bode's plot. The data also supports the inhibitor's progressive adsorption on the zinc surface. This blocks the sites that are active and lowers the extent of corrosion.[26] The Bode graphs (Fig. 4B) demonstrate that the impedance module $|Z|$ shifts towards larger values in comparison to the blank when CDZ is present. This displacement was caused by the adsorption of the CDZ drug on the zinc surface.[56] Consequently, the assessed CDZ slowed down the kinetics of the zinc corrosion in HCl medium.[70] Fig. 4B shows that for the Bode plots at the mid-frequency range, $\log Z$ and $\log f$ have a direct proportionality. Also, the phase angle value is near −60°, and the slope approaches −1. This verifies the inadequate capacitive performance at intermediate frequencies.[58] Perfect capacitive performance was attained at moderate frequencies when the slope is −1 and the angle of phase is −90°. Compared to uninhibited solutions, inhibited solutions have larger slope and phase angle magnitudes. This makes clear how efficiently the drug under investigation inhibits zinc degradation.[57]

Adapting the results of EIS studies with the described circuit in Fig. 4C allows one to examine the impedance spectra. Table 5 shows the impedance parameters, which include the double layer capacitance (C_{dl}), inhibition efficiency (IE_{EIS}), and charge transfer resistance (R_{ct}). When CDZ concentration increases, R_{ct} and IE_{EIS} values increase, indicating that a shielding film has developed on the metal/solution interface.[68,70] The C_{dl}, was inversely proportional to R_{ct} based on the following equation.

$$C_{dl} = \frac{1}{2\pi} f_{max} R_{ct} \tag{11}$$

where f_{max} represents the frequency at which the imaginary part of the impedance is at its highest value. In the presence of CDZ medication, the C_{dl} values decreased (Table 5). This results from an increase in the thickness of the double layer surrounding the shielding film and/or a decrease in the local dielectric constant caused by the deposited CDZ molecules permuting the H_2O molecules at the Zn surface.[68] The effective adsorption mechanism may be the cause of the decreased C_{dl} values with increasing CDZ medication additions. This finding implies that the drug

Table 5 EIS data of zinc in 1 mol per L HCl without and with different concentrations of the Ceftazidime drug at 298 K

[CDZ] (ppm)	R_{ct} (Ω cm^2)	C_{dl} ×10^{-6} (F cm^{-2})	θ	IE_{EIS} (%)
Blank	110.6	348	—	—
50	179.2	100.2	0.383	38.3 ± 0.2
100	211.3	83.6	0.477	47.7 ± 0.1
150	255.2	65.8	0.567	56.7 ± 0.1
200	288.5	56.2	0.617	61.7 ± 0.3
250	311.8	48.5	0.645	64.5 ± 0.1
300	352.0	42.1	0.686	68.6 ± 0.4

Open Access Article. Published on 19 March 2025. Downloaded on 3/14/2026 12:22:18 PM.
This article is licensed under a Creative Commons Attribution-NonCommercial 3.0 Unported Licence.

molecules may initially cover the active centers on the zinc surface by adsorption.[71] Using the following equation,[72] the inhibition efficiency values (Table 4) can be calculated from the R_{ct} values.

$$IE_{EIS} = \frac{R_{ct} - R_{ct}^{\circ}}{R_{ct}} \times 100 \quad (12)$$

where R_{ct} and R_{ct}° stand for Zn's electric charge transfer resistance in blank solution with and free of CDZ, respectively. As the concentration of CDZ increases, the values of IE_{EIS} increase, reaching an efficiency of 68.6% at 300 ppm and 298 K. The findings suggest that a more protective coating was formed on the zinc surface with the addition of CDZ. These findings

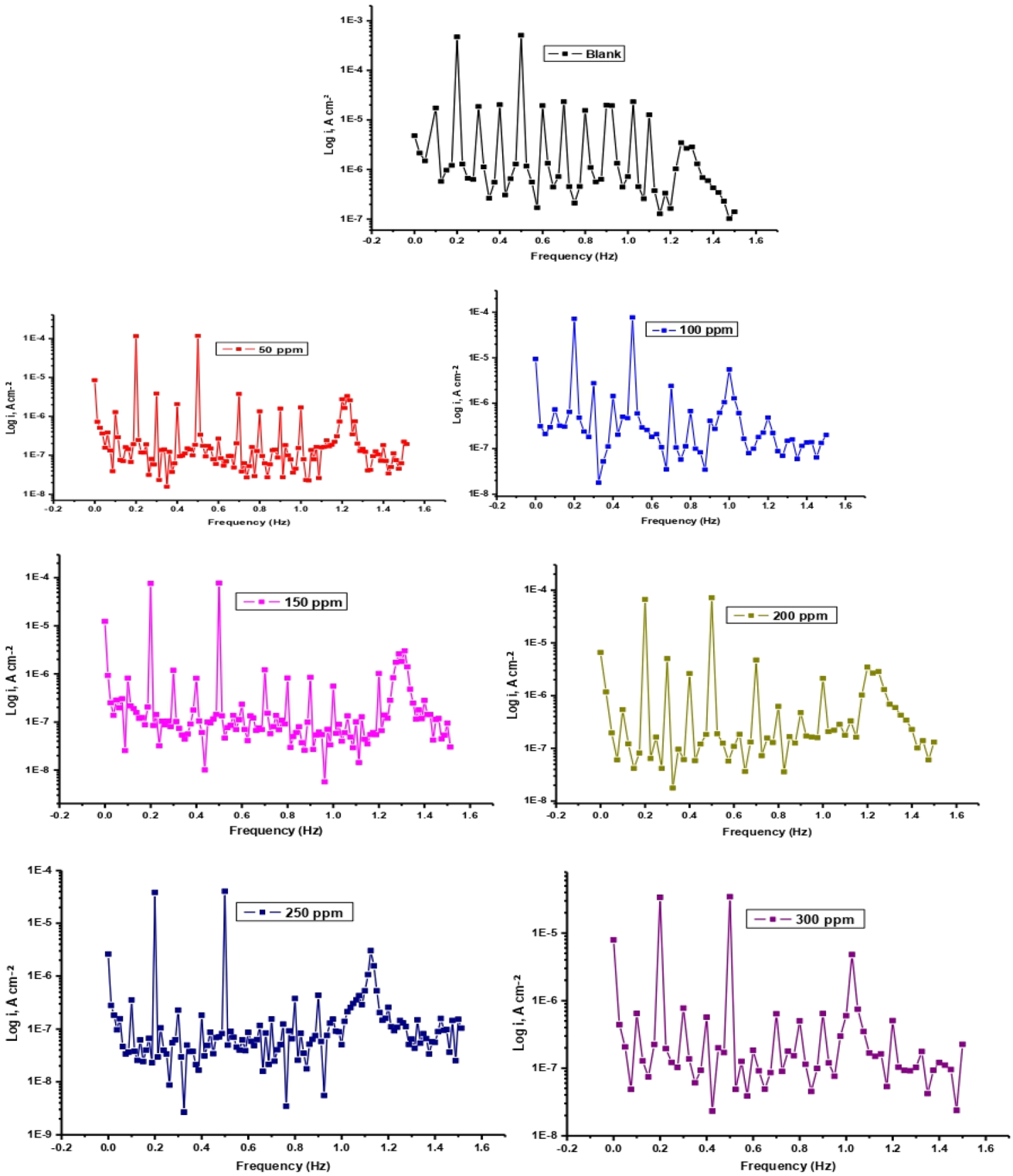

Fig. 5 EFM spectra for the corrosion of zinc in the blank solution without and with different concentrations of Ceftazidime drug at 298 K.

 © 2025 The Author(s). Published by the Royal Society of Chemistry

Open Access Article. Published on 19 March 2025. Downloaded on 3/14/2026 12:22:18 PM.
This article is licensed under a Creative Commons Attribution-NonCommercial 3.0 Unported Licence.

Table 6 Electrochemical kinetic parameters obtained by the EFM technique for zinc metal in 1 mol per L HCl in the absence and presence of different concentrations of the expired Ceftazidime drug at 298 K

[CDZ] (ppm)	i_{corr} ×10^{-6} (A cm^{-2})	$\beta_a \times 10^{-3}$ (V dec^{-1})	$-\beta_c \times 10^{-3}$ (V dec^{-1})	CF-2	CF-3	IE_{EFM} (%)
Blank	265	91	323	1.92	2.93	—
50	163.5	73.2	188.8	1.82	2.87	38.3 ± 0.1
100	135.1	71.4	129.2	1.89	3.12	49.0 ± 0.2
150	110.2	55.1	110.5	1.95	3.10	58.4 ± 0.3
200	99.8	52.2	87.5	1.87	3.09	62.3 ± 0.1
250	85.2	45.9	59.2	2.10	2.89	67.8 ± 0.2
300	78.7	41.2	57.4	2.03	2.85	70.3 ± 0.3

validate the consistency between the outcomes from EIS and alternative methods.

3.5 EFM study

Several advantages of the EFM technique, including direct, nondestructive, quick corrosion rate measurement and data validation, make it a perfect choice for online corrosion monitoring applications.[51] The EFM approach is a small signal AC technique that resamples the EIS. On the other hand, two distinct sine waves are applied simultaneously in this technique. Since there can be no direct relationship (non-linear) between I and V, the examined system responds to the excitation potential non-linearly.[42] As seen in Fig. 5, the input frequencies as well as their frequency components were considered in the current response. The frequency constituents are the sum of the two input frequencies, as well as their

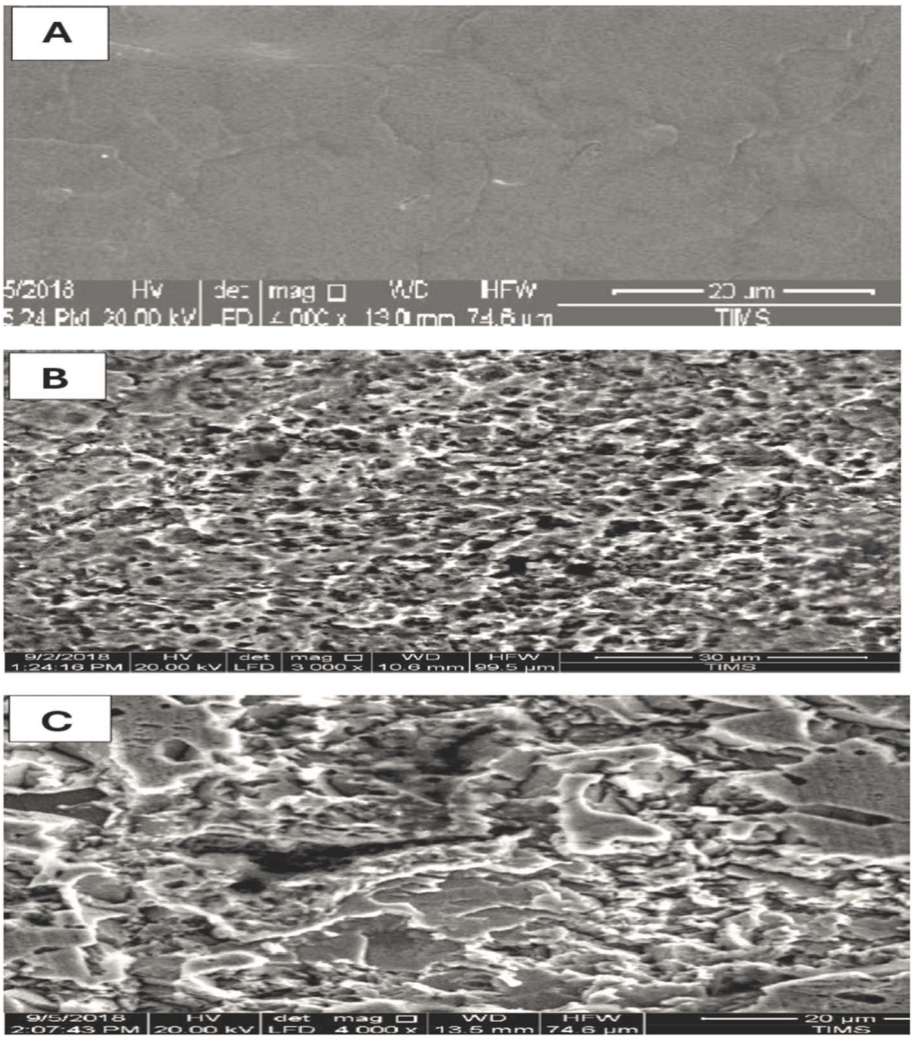

Fig. 6 SEM micrographs of polished zinc (A), zinc after 8 h immersion in a 1 mol per L Cl without (B), and with (C) 300 ppm of expired Ceftazidime drug at 298 K.

Open Access Article. Published on 19 March 2025. Downloaded on 3/14/2026 12:22:18 PM.
This article is licensed under a Creative Commons Attribution-NonCommercial 3.0 Unported Licence.

multiples and differences. The EFM diagrams of the zinc metal, under study, in a blank solution having varying dosages of the CDZ medication at 298 K are shown in Fig. 5. Because of the excitation frequencies, there are two prominent peaks at 0.2 and 0.5 Hz. The larger peaks were used to compute the slopes of Tafel, the causality factors (CF2 and CF3), and the corrosion

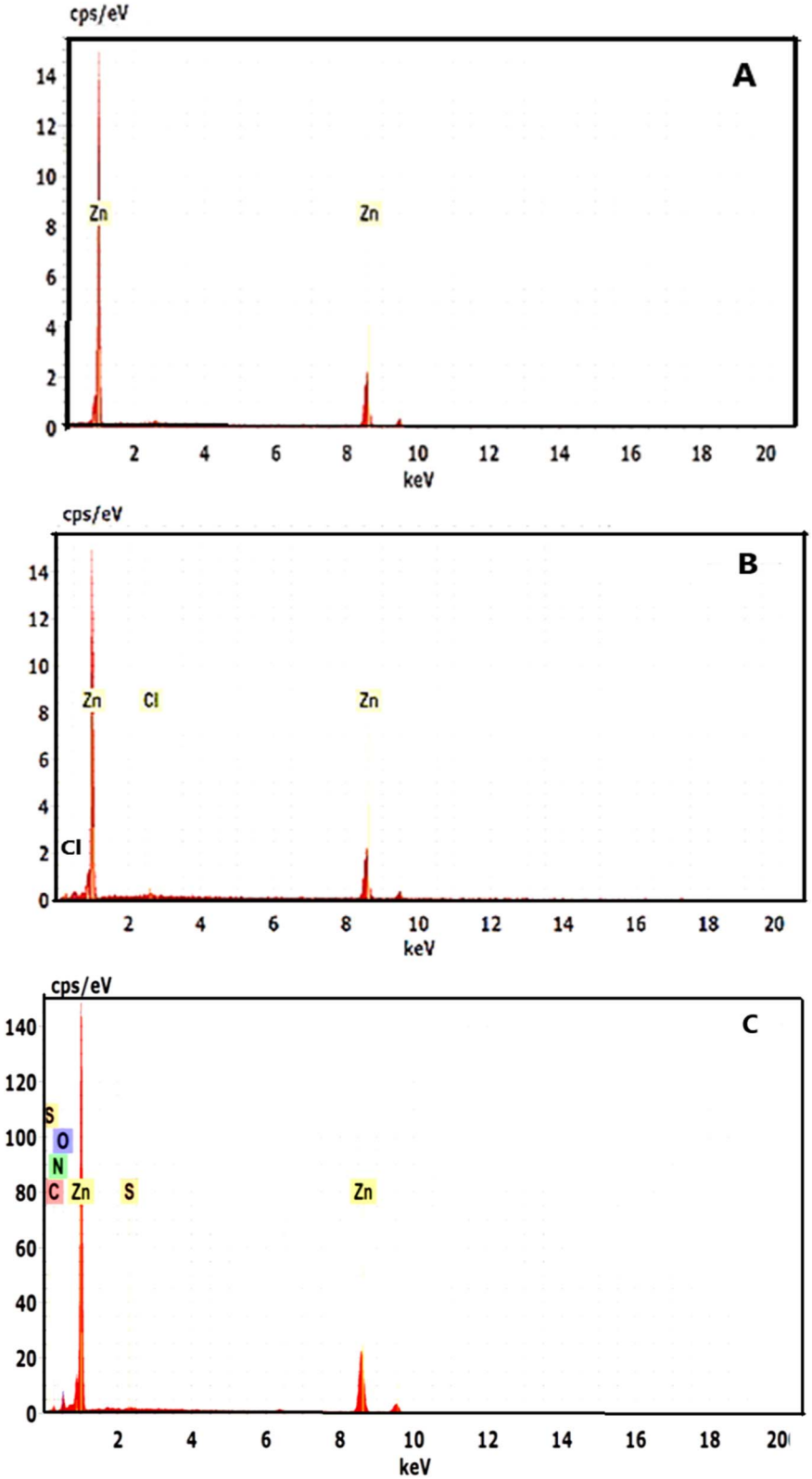

Fig. 7 EDX spectra of polished zinc (A), zinc after 8 h immersion in a 1 mol per L HCl without (B), and with (C) 300 ppm of expired Ceftazidime drug at 298 K.

 © 2025 The Author(s). Published by the Royal Society of Chemistry

Open Access Article. Published on 19 March 2025. Downloaded on 3/14/2026 12:22:18 PM.
This article is licensed under a Creative Commons Attribution-NonCommercial 3.0 Unported Licence.

current (i_{corr}). The kinetic features of the corrosion process, such as inhibition efficiency (IE_{EFM}), i_{corr}, Tafel parameters, and causality factors, are shown in Table 6. The insertion of the expired CDZ drug into the blank solution resulted in a reduction in the i_{corr} of zinc metal. Increasing the concentration of CDZ from 50 to 300 ppm reduces the corrosion current density from 163.5 to 78.7 μA cm^{-2}. This is likely due to the adsorption of the drug molecules onto the zinc surface. The CDZ acts as a barrier and inhibits the corrosion process.[42]

The efficiency of the inhibition (IE_{EFM}) increases with Ceftazidime concentration. According to Table 6, the causality factors closely resemble the ones that were predicted. This might ensure that the different parameters and corrosion current densities are accurate, according to EFM theory.[68] With the EFM data as a basis, eqn (13) computes IE_{EFM}.

$$IE_{EFM} = \frac{i^{\circ}_{corr} - i_{drug}}{i^{\circ}_{corr}} \times 100 \quad (13)$$

where i°_{corr} and i_{drug} stand for the corrosion current densities without and with CDZ drug, respectively.

3.6 SEM and EDX examinations

Using the SEM technique, it was possible to determine whether the zinc surface had a protective film from the expired CDZ. Moreover, EDX analyses were conducted to ascertain whether the medication is adsorbed on the zinc surface or not. Fig. 6 displays SEM photographs of the cleaned zinc surface and the zinc surface after submerging in a blank solution free of and with 300 ppm of the medication CDZ. The polished zinc surface is smooth and compact without any defects (Fig. 6A). The SEM micrographs for the zinc surface after 8 hours submersion in a blank solution free of and with 300 ppm of CDZ medication are displayed in Fig. 6B and C, respectively. The SEM image (Fig. 6B) of the corroded zinc sample in 1 mol per L HCl solution reveals a badly damaged zinc surface covered by corrosion products. Smaller pits evenly spread laterally and internally may have led to the extended corrosion region. On the other hand, zinc metal corrosion is significantly suppressed when the CDZ medication is present (Fig. 6C). Consequently, the presence of the CDZ medication on the zinc surface lowers the rate at which it dissolves in the HCl medium.

To confirm that the CDZ medication molecules are present on the zinc surface, EDX analysis is used. Fig. 7 shows the corresponding EDX spectra. Zinc peaks were the only ones found for the polished zinc sample (Fig. 7A). Because $ZnCl_2$ forms at the zinc surface in the presence of the blank solution, there were peaks for both zinc and chloride elements (Fig. 7B).[53] As seen in Fig. 7C, there were peaks for C, S, N, and O elements in the EDX spectrum for zinc coupons subjected to the CDZ drug. This result demonstrates that the medication was adsorbed onto the zinc surface, significantly impeding the zinc's ability to dissolve in the HCl solution.[42]

3.7 Computations involving quantum chemistry

3.7.1 DFTB simulations. Significant details concerning the electronic and thermodynamic characteristics of corrosion-inhibitory compounds can be obtained by Density Functional Tight-Binding (DFTB) simulations. The DFTB method was used to assess the frontier molecular orbitals (FMOs) of CDZ (Fig. 8), which comprise the highest occupied (HOMO) and lowest unoccupied (LUMO) molecular orbitals. The pyridinium-1-ylmethyl group that lies at the 3-position of the antibiotic's cephem ring contains the HOMOs of CDZ. On the other hand, LUMOs are positioned at the two oxygens of the carboxylic group.

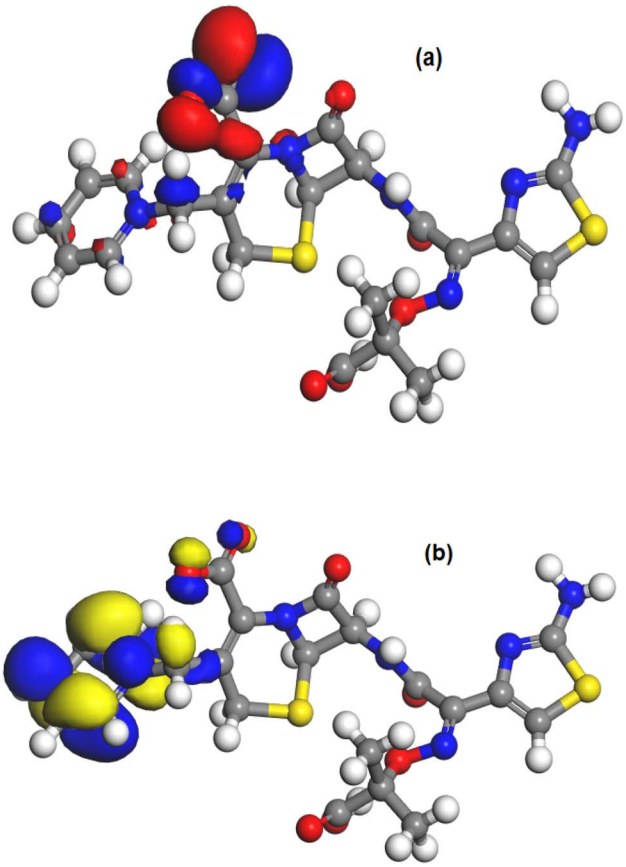

Fig. 8 FMO diagram of Ceftazidime (a) LUMO and (b) HOMO.

According to the results, the HOMO and LUMO energies were −5.833 and −3.381, respectively. With a computed energy

Table 7 The calculated quantum chemical parameters, obtained from DFTB data

Parameter (au)	Value
Energy of highest occupied molecular orbital (E_{HOMO})	−5.833
Energy of lowest unoccupied molecular orbital (E_{LUMO})	−3.381
Energy gap (ΔE)	2.452
Chemical hardness (η)	1.226
Chemical softness (σ)	0.816
Chemical potential (μ)	−4.607
Electronegativity (χ)	4.607
Electron affinity (A)	3.381
Ionization potential (I)	5.833
Electrophilicity index (ω)	8.656
Maximum charge transfer index (ΔN_{max})	3.758
Nucleophilicity (ε)	0.116

Open Access Article. Published on 19 March 2025. Downloaded on 3/14/2026 12:22:18 PM.
This article is licensed under a Creative Commons Attribution-NonCommercial 3.0 Unported Licence.

gap (ΔE) of 2.452, CDZ exhibited good stability and the ability to successfully reduce corrosion (Table 7). The metal's surface binding capability can be increased by decreasing the inhibitor's ΔE value, which will increase the reactivity between the metal and the inhibitor molecule. This increase in binding capacity may lead to an improvement in the inhibition efficiency of the compound because less energy is required to liberate the electron from the HOMO orbital.[73]

Electrostatic potential (ESP) maps assist in offering a better understanding of the electron-rich and electron-deficient regions of molecules.[74] The red areas (negative portions) of the map indicate places that support an electrophilic attack, whereas the blue regions (positive portions) of the map indicate sites that support a nucleophilic attack (Fig. 9). A light blue area refers to a slightly electron-deficient location; the yellow area indicates a slightly electron-rich position, and the green area indicates a neutral location. The ESP map of the CDZ compound showed that the pyridinium-1-ylmethyl group acts as a nucleophile (red to orange areas); on the other hand, the carboxylic group functions as an electrophile (blue area). The hydrophobic carbon chain repelled serious pitting chloride ions away from the zinc surface, facilitating the adhesion of adsorbed molecules.[75]

DFTB data can be used to compute a few descriptors that evaluate the CDZ drug's inhibitory performance. The energies of the highest occupied (E_{HOMO}) and the lowest unoccupied (E_{LUMO}) molecular orbitals can be used to calculate them. The energy gap (ΔE), ionization potential (I), electron affinity (A), chemical potential (μ), electronegativity (χ), hardness (η), softness (σ), electrophilicity index (ω), nucleophilicity (ε), and a proportion of electron transfer (ΔN_{max}) are reported in Table 7, which is based on the literature.[76] According to the following relations, the parameters are computed.[77]

$$\Delta E = E_{LUMO} - E_{HOMO} \tag{14}$$

$$I = -E_{HOMO} \tag{15}$$

$$A = -E_{LUMO} \tag{16}$$

$$\mu = -\chi \tag{17}$$

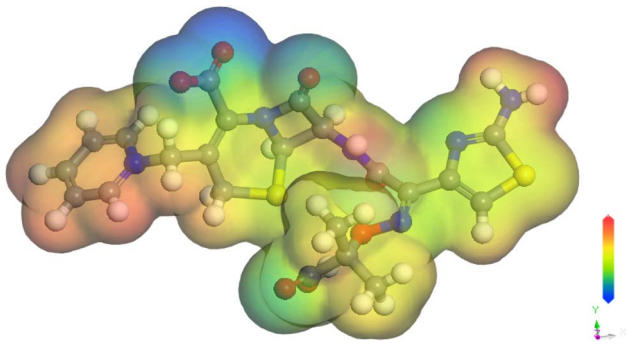

Fig. 9 Electrostatic potential map of Ceftazidime molecule.

$$\mu = \frac{(E_{HOMO} + E_{LUMO})}{2} \tag{18}$$

$$\eta = \frac{(E_{LUMO} - E_{HOMO})}{2} \tag{19}$$

$$\sigma = 1/\eta \tag{20}$$

$$\Delta N_{max} = \frac{-\mu}{\eta} \tag{21}$$

$$\omega = \frac{\mu^2}{2\eta} \tag{22}$$

$$\varepsilon = 1/\omega \tag{23}$$

The chemical reactivity of molecules is indicated by their ionization potentials. Compared to high ionization potentials that indicate the high stability of the molecules, smaller values represent more activity for the molecules.[78] Due to its small ionization potential (5.833), CDZ has good inhibitory efficiency, as seen in Table 7. An important consideration when assessing the CDZ drug's responsiveness is its electronegativity (χ) value. The value of 4.607 refers to the degree to which it can hold electrons.[79] A substantial interaction between CDZ and the zinc metal was confirmed by a low value of softness and a big value of hardness.[80] The reactivity of the CDZ molecule is demonstrated by its electrophilicity (ω) value of 8.656. ε is nucleophilicity, which is the reciprocal of electrophilicity. With an estimated ΔN_{max} value of 3.758, CDZ is capable of releasing electrons and supports the development of a shielding layer on the zinc surface.[81] The computation studies show that the present drug has efficient adsorption centers that can readily adsorb on the zinc surface and create a protective layer.

3.7.2 Monte Carlo simulation studies. While electronic parameters are effective in describing the drug's mechanism of action, they are insufficient to figure out the trend of the drug's inhibitive performance.[82] Therefore, it is crucial to carry out detailed modeling of the drug's direct interactions with the Zn surface. Adsorption is thought to be the main way by which corrosion is inhibited. The nature of interactions between the investigated drug and the Zn (002) crystal surface in 1 mol per L HCl was thus established by simulating the adsorption of the CDZ compound on the Zn surface. Because it possesses the most stable surface, the Zn (002) surface is utilized for the MC simulation study.

Using an MC simulation, Fig. 10 displays the drug's most stable low-energy adsorption configuration on Zn (002). Through the process of adsorption, the drug forms a protective film on the zinc surface. The film protects the zinc surface and keeps the corrosive solution away from it. Table 8 shows the values of the adsorption, the deformation, and the rigid adsorption energies for the adsorption of the CDZ drug on the Zn (002) surface. The adsorption energy of -77.41 kJ mol^{-1} indicates a significant interaction between the CDZ molecule and the zinc surface. This suggests that the drug is likely to bind effectively to the metal.[24] The deformation energy of

 © 2025 The Author(s). Published by the Royal Society of Chemistry

Open Access Article. Published on 19 March 2025. Downloaded on 3/14/2026 12:22:18 PM.
This article is licensed under a Creative Commons Attribution-NonCommercial 3.0 Unported Licence.

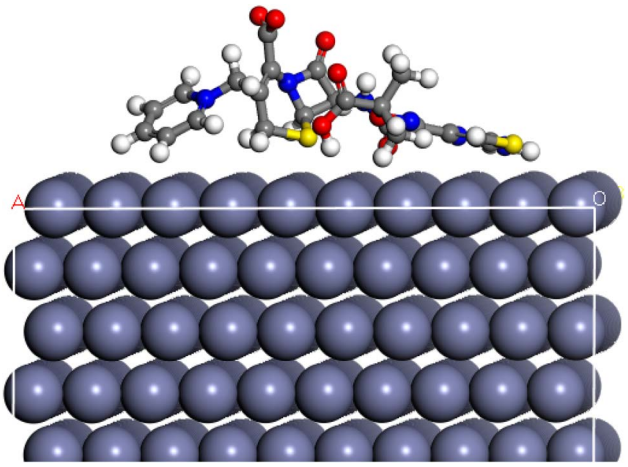

Fig. 10 The side view of the adsorption of the Ceftazidime drug on the zinc surface.

1.88 kJ mol^{-1} suggests that the CDZ molecule undergoes a slight conformational change upon adsorption. This is expected as the molecule needs to adjust its shape to optimize its interaction with the surface. The rigid adsorption energy of −79.29 kJ mol^{-1} provides an estimate of the adsorption energy without considering the conformational changes of the molecule. Comparing this value to the adsorption energy suggests that the deformation energy has a minor impact on the overall adsorption strength.

Eqn (24) is used to compute the adsorption energy, or E_{ads}.

$$E_{ads} = E_{Zn\text{-}inh} - (E_{inh} - E_{Zn}) \quad (24)$$

where E_{Zn} is the zinc surface's total energy, and E_{inh} is the inhibitor's total energy. The surface energy of zinc (002) is zero.[83] Given the strong adsorption energy (−77.41 kJ mol^{-1}) and the relatively small deformation energy (1.88 kJ mol^{-1}); it is likely that the CDZ molecule adopts a relatively flat configuration on the zinc surface. This would maximize the contact area between the molecule and the metal, leading to stronger interactions. This enables the transfer of the lone pair of electrons of the heteroatoms and π-electrons from the pyridinium ring of the drug to the zinc metal.[84] The side view orientation could be influenced by specific interactions between functional groups on the CDZ molecule and the zinc surface. For example, the carboxylate group (–COO–) in CDZ might interact favorably with the zinc atoms due to electrostatic interactions. The CDZ molecule has two sulfur atoms. Sulfur atoms have relatively lower electronegativities, enabling relatively stronger coordinate bonding with surface metallic atoms. Many investigators reported the high inhibition efficiency of sulfur compounds.[85] Heteroatoms' inhibitory effect followed their inverse electronegativity order, which is S > N > O. Higher inhibition efficiency and more charge transfer are associated with lower electronegativity. Because these heteroatoms are protonated and exist in their cationic forms in acidic solutions,[85] they were adsorbed by means of the electrostatic force of attraction during the initial stages of the interaction.

3.8 Mechanism of inhibition

The dissolution and dissociation of Zn metal in the anodic region and the reduction of O_2 gas in the cathodic region are both impacted by the introduction of the CDZ medication to the acidic medium, as indicated by the values of E_{corr}, β_a, and β_c in Table 4. The values of the Tafel cathodic and anodic constants decrease when the dosage of the CDZ drug in the acidic blank solution increases. Since the expired medication slows down both the cathodic and anodic reactions, it is confirmed to function as a mixed inhibitor.[24] Such impacts might result from CDZ molecules adhering to the zinc surface.[63]

Table 3 shows that the computed values of ΔG°_{ads} are −21.97 to −30.49 kJ mol^{-1}, which indicates that the drug under study binds to zinc metal by chemisorption and physisorption.[56–58] The drug's interaction with the zinc surface could be due to the existence of COO^-, N, O, S, and π-electrons in its structure. At the cathode, O_2 and H^+ ions in the solution combine to make H_2O, while at the anode, Zn metal is ionized to Zn^{2+} (en (3)). While the absence of vacant d-orbitals in zinc might seem to limit its ability to chemisorb, other mechanisms like s–p hybridization,[86] electrostatic interactions,[87] and charge transfer[88] can still lead to strong adsorption. Furthermore, the CDZ molecule retro-donates electrons from the zinc metal *via* the carboxylic group's two oxygens (LUMO orbital).[24] In addition, a protective coating is established on the Zn surface *via* physisorption between the protonated CDZ molecules and the Cl^- ions in the corrosive environment.[40] The film inhibits further zinc oxidation and decreases the metal's surface area in contact with the corrosive solution.[24] Fig. 11 shows the suggested mechanism of inhibition.

3.9 A comparison of the previously mentioned drugs with the expired Ceftazidime drug

In Table 9, the performance of the expired Ceftazidime drug under examination towards zinc protection is compared with other corrosion-inhibiting drugs published in the literature. According to this comparison, the expired CDZ is a good inhibitor and can be used to protect zinc metal in a 1 mol per L HCl medium.

Table 8 The adsorption, the deformation, and the rigid adsorption energies for the adsorption of the Ceftazidime drug on the Zn (002) surface

Total energy (kJ mol^{-1})	Adsorption energy (kJ mol^{-1})	Deformation energy (kJ mol^{-1})	Rigid adsorption energy (kJ mol^{-1})
680.25	−77.41	1.88	−79.29

Open Access Article. Published on 19 March 2025. Downloaded on 3/14/2026 12:22:18 PM.
This article is licensed under a Creative Commons Attribution-NonCommercial 3.0 Unported Licence.

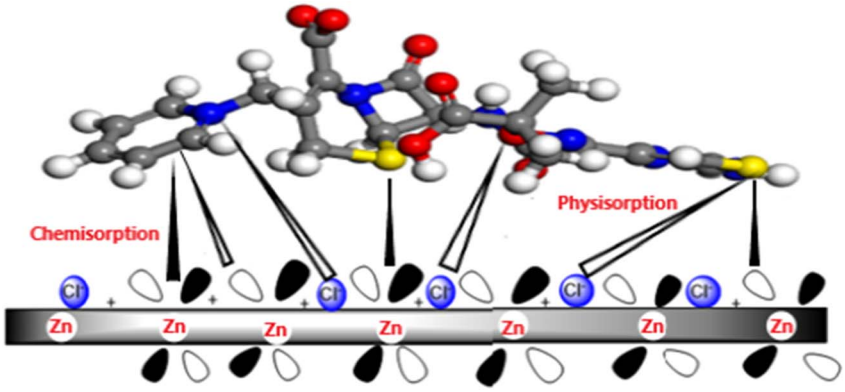

Fig. 11 Proposed mechanism of the Ceftazidime drug as a corrosion inhibitor for zinc metal.

Table 9 The comparison between other drugs and the tested expired Ceftazidime

The drug	The corrosive medium	Inhibition efficiency	Reference
Pentoxifylline	0.1 M HCl at 298 K	84.3% at 300 ppm	89
Expired cefazolin	0.5 M HCl at 298 K	87.3% at 300 ppm	24
Expired glycyrrhizin	0.5 M H_2SO_4 at 298 K	93.6% at 500 ppm	90
Expired gatifloxacin	3.5% NaCl at 298 K	87.0% at 500 ppm	91
Expired levofloxacin	3.5% NaCl at 298 K	89.0% at 500 ppm	91
Expired amiodarone	1.0 M HCl at 298 K	88.8% at 0.001 M	92
Expired hemorheologic	0.1 M HCl at 303 K	84% at 300 ppm	30
Telmisartan	0.1 M HCl at 298 K	77.0% at 20 ppm	32
Expired gabapentin	0.1 M HCl at 298 K	85.0% at 400 ppm	37
Hexamine	0.15 M HCl at 301 K	62.0% at 0.01M	6
Expired Ceftazidime	1.0 M HCl at 298 K	70.3% at 300 ppm	This work

4. Conclusions

In this study, Ceftazidime, an expired drug, was successfully reused to reduce zinc metal corrosion in a 1 mol per L hydrochloric acid solution. FTIR spectroscopy showed no significant change in chemical structure between fresh and expired drugs. The performance of the CDZ drug was examined using PDP, EFM, WL, and EIS methods. The WL method, the EFM, PDP, and EIS techniques showed good agreement. In a 1 mol per L HCl medium, CDZ inhibited zinc corrosion well. The inhibition performance improved with increasing CDZ drug concentration, reaching 70.3% efficacy at 300 ppm, while it was reduced at higher temperatures. Concentrations above 300 ppm failed to enhance the inhibition effect. The inhibition is caused by expired drug adsorption on the zinc surface. The adsorption behavior was consistent with the Temkin model. ΔG°_{ads} have negative values below 40 kJ mol^{-1}. The thermodynamic data indicated that the drug was absorbed both physically and chemically, establishing a protective film on the zinc surface. Ceftazidime is classified as a mixed-type inhibitor. The adsorption of CDZ medication on the zinc surface reduced the corrosion rate, as demonstrated by SEM and EDX analyses. The DFTB and MC simulation findings showed that the expired medication attached to the zinc surface by the heteroatoms' lone pair of electrons. In addition to the pyridinium ring's π-electrons. The drug's adsorption energy with the zinc surface was −77.41 kJ mol^{-1}. Zinc metal in HCl medium can be protected by using an expired Ceftazidime drug, which is an effective inhibitor.

Data availability

Data will be made available on request.

Conflicts of interest

The authors declare that they have no known competing financial interests or personal relationships that could have appeared to influence the work reported in this paper.

Acknowledgements

The authors extend their appreciation to Taif University, Saudi Arabia, for supporting this work through project number (TU-DSPP-2025-19).

References

1 M. J. Mazumder, *Glob. J. Eng. Sci.*, 2020, **5**, 1–5.
2 A. Kellenberger, D. A. Duca, M. L. Dan and M. Medeleanu, *Materials*, 2022, **15**, 2918.
3 H. Kania and M. Saternus, *Appl. Sci.*, 2023, **13**, 2003.

 © 2025 The Author(s). Published by the Royal Society of Chemistry

Open Access Article. Published on 19 March 2025. Downloaded on 3/14/2026 12:22:18 PM.
This article is licensed under a Creative Commons Attribution-NonCommercial 3.0 Unported Licence.

4 A. Pola, M. Tocci and F. E. Goodwin, *Metals*, 2020, **10**, 253.
5 G. A. Gaber, A. Y. Hassan, M. S. Kadh, N. M. Saleh, E. S. Abou-Amra and A. M. Hyba, *Chem. Pap.*, 2024, **78**, 3189–3203.
6 R. T. Vashi, *Int. J. Res. Appl. Sci. Eng. Technol.*, 2020, **8**, 128–135.
7 M. B. Mahida and H. G. Chaudhari, *Der Pharm. Chem.*, 2012, **4**, 2305.
8 A. V. Shanbhag, T. V. Venkatesha, R. A. Prabhu and B. M. Praveen, *Bull. Mater. Sci.*, 2011, **34**, 571–576.
9 M. D. Shah, A. S. Patel, G. V. Mudaliar and N. K. Shah, *Port. Electrochim. Acta*, 2011, **29**, 101–113.
10 N. Hebbar, B. M. Praveen, B. M. Prasanna and V. T. Venkatesha, *Trans. Indian Inst. Met.*, 2015, **68**, 543–551.
11 M. M. Solomon, S. A. Umoren, I. I. Udosoro and A. P. Udoh, *Corros. Sci.*, 2010, **52**, 1317–1325.
12 S. Ade, S. Nana and S. M. Lonkar, *Int. J. ChemTech Res.*, 2014, **6**, 3642–3650.
13 G. Karthik and M. Sundaravadivelu, *Egypt. J. Pet.*, 2016, **25**, 183–191.
14 S. Karthikeyan, *Int. J. ChemTech Res.*, 2016, **9**, 251–259.
15 R. S. A. Hameed, H. I. AlShafey and A. H. Abu-Nawwas, *Int. J. Electrochem. Sci.*, 2014, **9**, 6006–6019.
16 A. S. Fouda, M. N. EL-Haddad and Y. M. Abdalla, *Int. J. Innovat. Stud. Sci. Eng. Technol.*, 2013, **2**(12), 7073.
17 K. A. Yasakau, A. Kuznetsova, H. M. Maltanava, S. K. Poznyak, M. G. S. Ferreira and M. L. Zheludkevich, *Corros. Sci.*, 2024, **229**, 111889.
18 Y. Ouyang, Y. Wei, R. Zhang, R. Li, Z. Lin, S. Shi and R. Qiu, *Colloids Surf. A Physicochem. Eng. Asp.*, 2024, **681**, 132779.
19 M. Abdallah, E. A. M. Gad, M. Sobhi, J. H. Al-Fahemi and M. M. Alfakeer, *Egypt. J. Pet.*, 2019, **28**, 173–181.
20 N. Vaszilcsin, V. Ordodi and A. Borza, *Int. J. Pharm.*, 2012, **431**, 241–244.
21 S. Hooshmand Zaferani, M. Sharifi, D. Zaarei and M. R. Shishesaz, *J. Environ. Chem. Eng.*, 2013, **1**, 652–657.
22 D. Gikonyo, A. Gikonyo, D. Luvayo and P. Ponoth, *Afr. Health Sci.*, 2019, **19**, 2737–2739.
23 N. Vaszilcsin, A. Kellenberger, M. L. Dan, D. A. Duca and V. L. Ordodi, *Materials*, 2023, **16**, 5555.
24 R. A. Alsaiari, M. M. Kamel and M. M. Mohamed, *Molecules*, 2024, **29**, 1157.
25 H. Adil, *J. Al. Nahrain. Univ.*, 2015, **18**(1), 60–65.
26 A. M. Guruprasad, H. P. Sachin, G. A. Swetha and B. M. Prasanna, *Int. J. Ind. Chem.*, 2019, **10**, 17–30.
27 A. M. Guruprasad, H. P. Sachin, G. A. Swetha and B. M. Prasanna, *Surf. Interfaces*, 2020, **19**, 100478.
28 N. Hebbar, B. M. Praveen, B. M. Prasanna and T. V. Venkatesha, *J. Fund. Appl. Sci.*, 2015, **7**, 271–289.
29 N. Hebbar, B. M. Praveen, B. M. Prasanna and T. V. Venkatesha, *Int. J. Ind. Chem.*, 2015, **6**, 221–231.
30 J. C. Abbar, G. A. Swetha and H. P. Sachin, *Colloids Surf., A*, 2022, **650**, 129518.
31 E. Yousif, Y.-F. Win, A. H. Al-Hamadani, A. A. Al-Amiery, A. A. H. Kadhum and A. B. Mohamad, *Int. J. Electrochem. Sci.*, 2015, **10**, 1708–1715.
32 G. A. Swetha and H. P. Sachin, *Chem. Data Collect.*, 2021, **32**, 100668.
33 M. Abdallah, I. A. Zaafarany and B. A. A. Jahdaly, *J. Mater. Environ. Sci.*, 2016, **7**(4), 1107–1118.
34 A. Alwash, D. H. Fadhil, A. Ali, F. Abdul-Hameed and E. Yousif, *Rasayan J. Chem.*, 2017, **10**, 922–928.
35 E. Stupnišek-Lisac, S. Podbršček and T. Sorić, *J. Appl. Electrochem.*, 1994, **24**, 779–784.
36 R. T. Vashi and D. Naik, *Asian J. Chem.*, 2010, **22**, 7761.
37 G. A. Swetha, H. P. Sachin and J. R. Choudhuri, *Emergent Mater.*, 2023, **6**, 721–740.
38 N. O. Eddy, S. A. Odoemelam, E. C. Ogoko and B. I. Ita, *Port. Electrochim. Acta*, 2010, **28**, 15–26.
39 G. Gece, *Corros. Sci.*, 2011, **53**, 3873–3898.
40 A. K. Singh, S. K. Shukla and M. A. Quraishi, *Int. J. Electrochem. Sci.*, 2011, **6**, 5802–5814.
41 A. K. Singh, S. K. Shukla, M. Singh and M. A. Quraishi, *Mater. Chem. Phys.*, 2011, **129**, 68–76.
42 M. M. Kamel, Q. Mohsen, Z. M. Anwar and M. A. Sherif, *J. Mater. Res. Technol.*, 2021, **11**, 875–886.
43 Z. G. Luo, Y. Zhang, H. Wang, S. Wan, L. F. Song, B. K. Liao and X. P. Guo, *Corros. Sci.*, 2024, **227**, 111705, DOI: 10.1016/j.corsci.2023.111705.
44 *Designation: G 1–03; Standard practice for preparing, cleaning, and evaluating corrosion test specimens*, ASTM International, West Conshohocken, PA, USA, 1990, pp. 19428–22959.
45 D. Frenkel and B. Smit, *Understanding Molecular Simulation: from Algorithms to Applications*, Elsevier, 2023.
46 M. Gatchell, M. Goulart, L. Kranabetter, M. Kuhn, P. Martini, B. Rasul and P. Scheier, *Phys. Chem. Chem. Phys.*, 2018, **20**, 7739–7745.
47 G. Zheng, H. A. Witek, P. Bobadova-Parvanova, S. Irle, D. G. Musaev, R. Prabhakar, K. Morokuma, M. Lundberg, M. Elstner, C. Köhler and T. Frauenheim, *J. Chem. Theory Comput.*, 2007, **3**, 1349–1367.
48 S. L. Muhammad and mad B. Ibrahim, *Bayero J. Pure Appl. Sci.*, 2022, **13**, 149–162.
49 O. Abakedi and J. Asuquo, *J. Basic Appl. Res. Biomed.*, 2016, **2**, 556–560.
50 M. A. Hegazy, *J. Mol. Liq.*, 2015, **208**, 227–236.
51 M. Bobina, A. Kellenberger, J.-P. Millet, C. Muntean and N. Vaszilcsin, *Corros. Sci.*, 2013, **69**, 389–395.
52 M. Pais and P. Rao, *J. Bio Tribo Corros.*, 2021, **7**, 117.
53 I. Abdelfattah, W. Abdelwahab and A. El-Shamy, *Egypt. J. Chem.*, 2022, **65**, 687–694.
54 H. M. Abd El-Lateef, V. M. Abbasov, L. I. Aliyeva, E. E. Qasimov and I. T. Ismayilov, *Mater. Chem. Phys.*, 2013, **142**, 502–512.
55 L. H. Abdel-Rahman and A. M. Abu-Dief, *Mater. Chem. Phys.*, 2013, **142**, 502–512.
56 M. M. Kamel, M. A. Ghanem, S. M. Rashwan, M. A. Mahmoud, S. A. El-Mekawy, K. M. H. Mohammed and H. E. Ibrahim, *RSC Adv.*, 2024, **14**, 19428–19445.
57 M. Kamel, M. Hegazy, S. Rashwan and M. El Kotb, *Chin. J. Chem. Eng.*, 2021, **34**, 125–133.
58 M. A. Hegazy, S. M. Rashwan, S. Meleek and M. M. Kamel, *Mater. Chem. Phys.*, 2021, **267**, 124697.
59 L. B. Furtado, R. C Nascimento, M. J. O. C. Guimarães, F. J. F. S. Henrique, J. C. Rocha, P. R. Seidl and

Open Access Article. Published on 19 March 2025. Downloaded on 3/14/2026 12:22:18 PM.
This article is licensed under a Creative Commons Attribution-NonCommercial 3.0 Unported Licence.

J. A. C. P. Gomes, *Sustainable Chem. Pharm.*, 2021, **19**, 100353.
60 T. S. Chu, W. J. Mai, H. Z. Li, B. X. Wei, Y. Q. Xu and B. K. Liao, *Int. J. Mol. Sci.*, 2025, **26**, 561, DOI: 10.3390/ijms26020561.
61 F. Bentiss, M. Lebrini and M. Lagrenée, *Corros. Sci.*, 2005, **47**, 2915–2931.
62 M. A. Migahed, S. M. Rashwan, M. M. Kamel and R. E. Habib, *Cogent Eng.*, 2017, **4**, 1366255.
63 M. M. Kamel, M. A. Ghanem, A. S. Fouda, S. M. Rashwan, O. M. Abdelkader, N. Y. Mostafa and K. M. H. Mohammed, *Egypt. J. Chem.*, 2024, **67**, 413–427.
64 S. B. Aoun, *RSC Adv.*, 2017, **7**, 36688–36696.
65 A. D. Becke, in *Book of Abstracts, 212th ACS National Meeting*, Orlando, FL, August 25-29, 1996.
66 A. D. Becke, *Phys. Rev. A*, 1988, **38**, 3098–3100.
67 J. A. Syed, S. Tang, H. Lu and X. Meng, *Ind. Eng. Chem. Res.*, 2015, **54**, 2950–2959.
68 I. Sekine, M. Sanbongi, H. Hagiuda, T. Oshibe, M. Yuasa, T. Imahama, Y. Shibata and T. Wake, *J. Electrochem. Soc.*, 1992, **139**, 3167.
69 P. Arellanes-Lozada, V. Díaz-Jiménez, H. Hernández-Cocoletzi, N. Nava, O. Olivares-Xometl and N. V. Likhanova, *Corros. Sci.*, 2020, **175**, 108888.
70 B. S. Sanatkumar, J. Nayak and A. Nityananda Shetty, *Int. J. Hydrogen Energy*, 2012, **37**, 9431–9442.
71 S. A. El Wanees, M. I. Alahmdi, M. A. Alsharif and Y. Atef, *Egypt. J. Chem.*, 2019, **62**, 811–825.
72 M. A. Amin, S. S. Abd El-Rehim, E. E. F. El-Sherbini and R. S. Bayoumi, *Electrochim. Acta*, 2007, **52**, 3588–3600.
73 U. T. Timothy, *J. Med. Nanomater. Chem.*, 2024, **6**, 81–94, DOI: 10.48309/jmnc.2024.1.7.
74 A. Thakur and A. Kumar, *Eur. J. Chem.*, 2023, **14**, 246–253.
75 A. Nasser, N. M. El Basiony, M. A. Migahed, H. M. Abd-El-Bary and T. A. Mohamed, *Egypt. J. Chem.*, 2022, **65**, 845–867.
76 M. Pais and P. Rao, *Chem. Pap.*, 2021, **75**, 1387–1399.
77 M. M. Kamel, S. M. Rashwan, M. A. A. Mahmoud, S. A. A. El-Mekawy, M. K. Awad and H. E. Ibrahim, *ACS Omega*, 2022, **7**, 17609–17619.
78 T. Chakraborty, K. Gazi and D. C. Ghosh, *Mol. Phys.*, 2010, **108**, 2081–2092.
79 A. Singh, K. R. Ansari, A. Kumar, W. Liu, C. Songsong and Y. Lin, *J. Alloys Compd.*, 2017, **712**, 121–133.
80 S. S. Al-Najjar and A. Y. Al-Baitai, *Phys. Chem. Res.*, 2022, **10**, 179–194.
81 N. Khalil, *Electrochim. Acta*, 2003, **48**, 2635–2640.
82 A. Bello, A. Uzairu and G. A. Shallangwa, *JOTCSA*, 2019, **6**, 451–462.
83 L. Guo, X. Ren, Y. Zhou, S. Xu and Y. Gong, Monte Carlo simulations of corrosion inhibition of copper by two Schiff bases, *Proceedings of the 2015 International Conference on Materials, Environmental and Biological Engineering*, Atlantis Press, 2015, pp. 622–625.
84 N. M. El Basiony, A. Elgendy, A. E. El-Tabey, A. M. Al-Sabagh, Gh. M. Abd El-Hafez, M. A. El-raouf and M. A. Migahed, *J. Mol. Liq.*, 2020, **297**, 111940.
85 Y. Qiang, H. Zhi, L. Guo, A. Fu, T. Xiang and Y. Jin, *J. Mol. Liq.*, 2022, **351**, 118638.
86 G. L. Miessler and D. A. Tarr, *Solutions Manual, Inorganic Chemistry*, Prentice Hall, 1999.
87 P. W. Atkins, J. D. Paula and J. Keeler, *Atkins' Physical Chemistry*, Oxford University Press, 2023.
88 D. P. Woodruff and T. A. Delchar, *Modern Techniques of Surface Science*, Cambridge University Press, Cambridge, 2nd edn, 1994. ISBN 0-521-42498-4.
89 J. C. Abbar, G. A. Swetha and H. P. Sachin, *Colloids Surf. A Physicochem. Eng. Asp.*, 2022, **650**, 129518.
90 Q. H. Chen, Z. Y. Zhou, M. T Feng, J. H. He, Y. Q. Xu and B. K. Liao, *J. Taiwan Inst. Chem. Eng.*, 2025, **168**, 105913.
91 A. Toghan, O. K. Alduaij, N. Alqarni, E. M. Masoud, H. Alhussain, A. M. Mostafa, A. A. Farag and A. Fawzy, *Results Chem.*, 2025, **13**, 102006.
92 H. M. K. Sheit, S. M. Kani, M. A. Sathiq, S. S. S. Abuthahir, P. Subhapriya, K. S. Nivedhitha, M. A. Umarfarooq, I. A. Badruddin, S. Kamangar and A. S. Shaik, *Materials*, 2024, **17**, 751, DOI: 10.3390/ma17030751.

 © 2025 The Author(s). Published by the Royal Society of Chemistry